Aero-acoustics in a tangential blower: validation of the CFD flow distribution using advanced PIV techniques

Jean-Yves Noël[1], Mark Farall[2] and Luca Casarsa[3]
[1]Electrolux Major Appliances Europe, Corso Lino Zanussi, 30 – 33080 Porcia (Italy)
[2]CD-adapco, 200 Shepherds Bush Road, London, W6 7NL, (United Kingdom)
[3]Dipartimento di Energetica e Macchine, Università degli Studi di Udine (Italy)
Contact Author: Jean-Yves Noël, Corso Lino Zanussi, 30 – 33080 Porcia (Italy)
E-mail: jean-yves.noel@electrolux.it

ABSTRACT

Noise reduction is of increasing importance in the community. Consequently, the development of aero-acoustics is gaining special focus within industry. Computational Aero-Acoustics (CAA), the coupling of Computational Fluid Dynamics (CFD) and Computational Acoustics (CA), is being used in the design and assessment of a range of products from HVAC ducts to domestic appliances.

The process for carrying out an Aero-Acoustic simulation begins with the solution of the transient flow dynamics in order to compute accurately the pressure fluctuations at a number of points in the computational domain. These fluctuations are passed to the acoustic code to propagate the acoustic waves through the system and determine its acoustic signature. To minimize errors in the acoustic propagation analysis it is thus essential that accurate predictions of the noise sources be obtained.

This paper concentrates on the CFD part of the aero-acoustic simulation. The case considered has been taken from the European project DESTINY:3 and comprises a tangential blower located inside a complex duct system. Air is drawn into the fan through two inlets and exits through a single duct. The computational methodology and flow field predictions are presented and compared to experimental PIV data. The numerical predictions were found to be in good agreement with the experimental data, reproducing the asymmetries in the flow field.

1. INTRODUCTION

Noise pollution is often rated highly in public surveys. As a result noise reduction has become an increasing focus for European Union legislation and a priority for research, as stated by a Strategy Paper update for the European Commission [1]. If this Strategy Paper clearly designates road, railway or air traffic and outdoor equipments as main noise emitters,

a change of public mindset is initiated and noise pollution is becoming a criterion when it comes to purchasing indoor equipment. As a consequence, industries such as home appliances or HVAC systems have started to seriously take into account the noise emission in the development of their products. The home appliance industry makes a large use of fans to increase the heat or the mass transfer: heat dissipation to cool down electronic components; uniform temperature distribution in a cooker or a fridge.

However, there is an associated noise with the use of fans, both by the impeller itself and by the air streams flowing through the ducts. Flow-induced noise or aero-acoustics is an example of a multi-physics problem. It is a discipline that studies the creation, the propagation and the scattering of sounds in fluids. The source of noise is the random fluctuation of the flow over a large range of frequencies (broadband noise), i.e. a pure fluid mechanic problem, while the propagation and scattering of the noise is a pure acoustic issue.

Numerical aero-acoustics couples two advanced modeling techniques: Computational Fluid Dynamics (CFD) and Computational Acoustics (CA).

The CFD will solve the full Navier-Stokes equation and take into account the turbulent flow while the acoustic code will calculate the propagation of the noise and determine the sound pressure levels. The information exchanged between the two codes is based on the Lighthill's analogy that has been deeply described and discuss in the literature [2, 3].

Aero-acoustic noise results from unsteady and turbulent flows. The choice of the turbulent model is therefore crucial as it conditions the quality of the information that will be passed to the acoustic code. Unsteady Reynolds Averaged Navier-Stokes (URANS) methods have been widely used [4] because of their reasonable computational cost but they are known to poorly predict the broadband noise [5]. Large Eddy Scale based models are definitively more suited for a correct computation of the turbulence [6] but the mesh requirements for the near-wall region lead to a significant increase of the computation cost and thus make it quite dissuasive for industrial use. An alternative is to use a Detached Eddy Simulation (DES) model which combines URANS properties (in the near-wall region) and LES away from walls [5, 7]. The computational cost of DES is more expensive than URANS but the overall increase doesn't exceed one order of magnitude [8].

The quality of the results is also strongly linked to the computational grid density and distribution. In general, the mean frequency of a cell is a function of the turbulent kinetic energy in that cell and its volume. Practically, the higher the frequency range needing to be resolved, the denser the grid. This clearly has a direct impact on the overall computation cost.

Due to the expected high computation cost and the required high quality of the information passed to the CA code, it is important to guarantee as early as possible in the workflow the quality of the CFD results.

This paper concentrates on the CFD part of the aero-acoustic workflow and its experimental verification with advanced techniques. A description of the test case is given in the second section, i.e. a tangential blower inserted in a system of ducts. Section 3 then describes the Computational Fluid Dynamics model and the main issues regarding the set-up. Few words are spent on the acoustic model that is built separately. Section 4 describes the Particle Image Velocimetry, a non-intrusive technique to measure flow over a given section. Finally, Section 5 presents the results of the study.

This work has been carried in the framework of the DESTINY:3 project.

2. CASE DESCRIPTION

The source of noise is a tangential blower comprising 22 blades as shown in figure 1. Each blade has a length of 180 mm and is mounted on metal rings at the extremities. To prevent the deflection of the blades, additional support is provided by a third metal ring located half

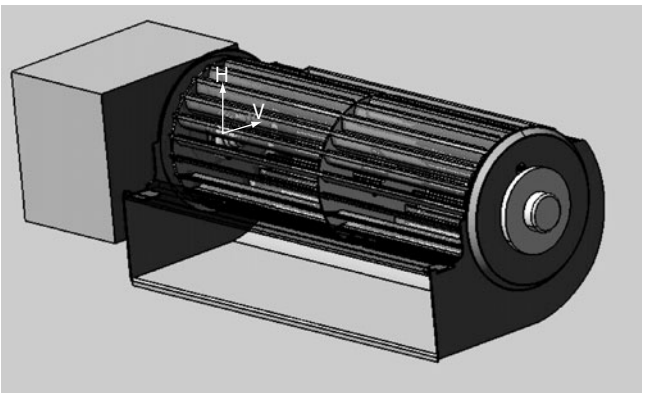

Figure 1 Geometrically simplified tangential blower in its casing and a simplified motor.

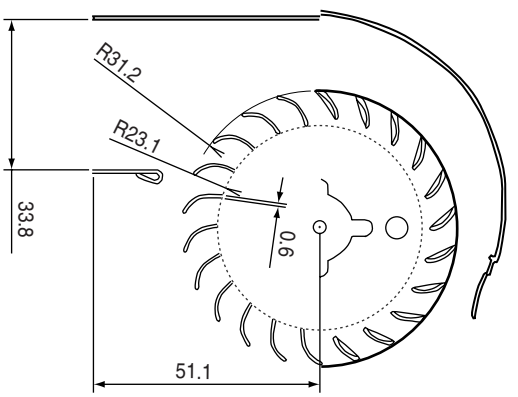

Figure 2 Cross section of the duct system perpendicular to the fan axis.

way along the blade length. The direction of rotation of the fan is such that the blades are curved forward. The external and internal diameters of the impeller are respectively 31.2 mm and 23.1 mm. Additional geometrical details are given in figure 2.

Figure 3 and 4 show the tangential blower and associated housing. The impeller is mounted in a horizontal duct separated into two parts across its width and length (see Figure 4). Flow enters the housing from two points; through the lower channel, called the "inflow channel", at a rate of 37.8 m^3hr^{-1} and from an opening in the rear volume of the housing at a rate of 58.9 m^3hr^{-1}. The flow exits the housing through the upper channel, named "exhaust channel". There is no interaction between the front inflow and outflow. The overall dimensions of the housing are 440 mm × 549 mm × 182 mm. It should be noted that the exhaust channel does not have a constant cross section: it is strongly diverging in the horizontal section and slightly converging in the vertical direction (see Figure 3). To increase optical access in prevision of the PIV measurements, the duct walls have been made with a transparent material.

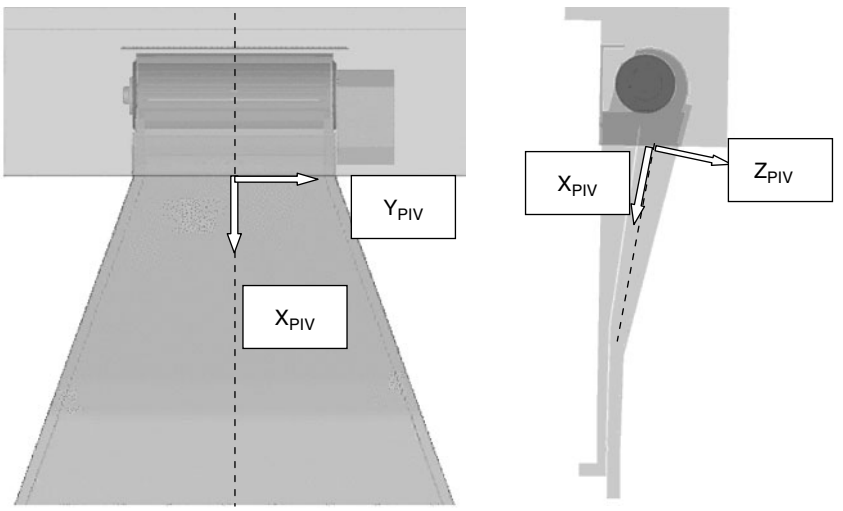

Figure 3 Duct system where the tangential blower is inserted.

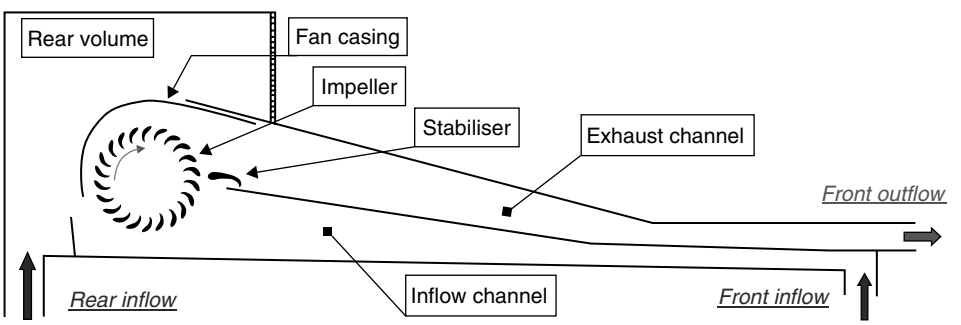

Figure 4 Cross section of the cross-flow impeller.

3. COMPUTATIONAL FLUID DYNAMICS

The turbulent flow generated by a fan is characterized by both broadband and narrowband noise. The former is associated with small-scale turbulent structures due to shearing of the flow while the latter with large periodic motions like vortex shedding or blade passing. The challenge for any simulation tool is to capture both types of motion at a sufficient resolution for the frequency range of interest.

All calculations in the present paper were performed with the general purpose thermofluids analysis code STAR-CD release 3.24.

3.1 COMPUTATIONAL MESH

The mesh comprises 2 regions, a rotating region incorporating the fan unit, and a stationary region (figure 5). These two regions were coupled via an extrusion layer (figure 6) such that the cells were matched on either side of the interface. To increase robustness of the meshing and solver process and keep a reduced number of cells, no extrusion layers were placed on the outer edges of the computational domain.

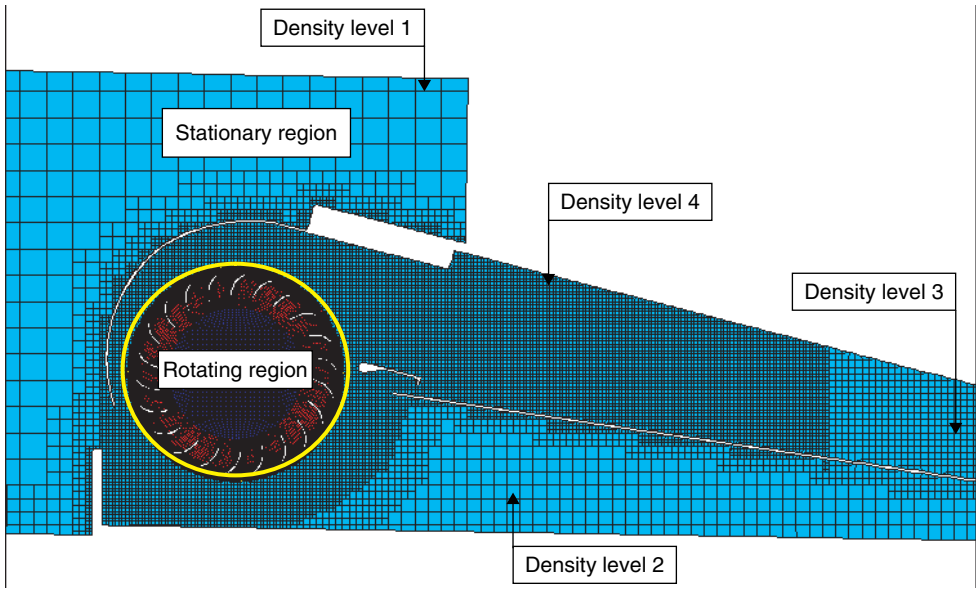

Figure 5 Overview of the main computational grid distribution with different densities.

The mesh density depends on the desired frequency range to be resolved. The current mesh has the higher density in the fan region with 55% of the total fluid cells and immediately downstream the fan unit where the main sources of noise was expected (figure 5).

Before performing a computationally expensive transient analysis, a steady state computation is performed for two reasons. The first one is to verify that a sufficient frequency range that can be resolved by the grid. Changes to the mesh can be carried out at this stage to ensure the expected range will be resolved. This is illustrated with figures 7 and 8 where the effects of two mesh densities on the frequency ranges were analyzed. An initial grid showed that a maximum frequency of 500 Hz could be resolved within the fan. A refined grid is guarantying to resolve frequencies over 1000 Hz in the whole rotating region while frequencies up to 700 Hz are captured in the cooling channel downstream the fan region. The second reason of running a steady state analysis is to provide an initial flow field for the transient calculation, reducing the computational time required to reach a limit cycled state of the model that is required before to extract any quantities for the aero-acoustic analysis itself.

To simulate the impeller, the steady state computation uses a Moving Reference Frame (MRF) approach while the transient calculation uses an explicit Sliding Mesh technique [9].

The final cell count for the present analysis was approximately 5.2 million.

3.2 THERMO-FLUID PROPERTIES

The working fluid was assumed to have the properties of air at standard atmospheric conditions:

- density: ideal gas law, with molecular weight of 28.96 g mol^{-1}
- molecular viscosity: $1.81 \cdot 10^{-5}$ kg m^{-1} s^{-1}

The flow was assumed to be single phase, three dimensional, compressible and fully turbulent. Transport equations were solved for the three momentum components, mass continuity, temperature and turbulent quantities.

Turbulence was modeled using the k-ε model for the steady state simulation and the k-ε Detached Eddy Simulation (DES) model for the transient analysis.

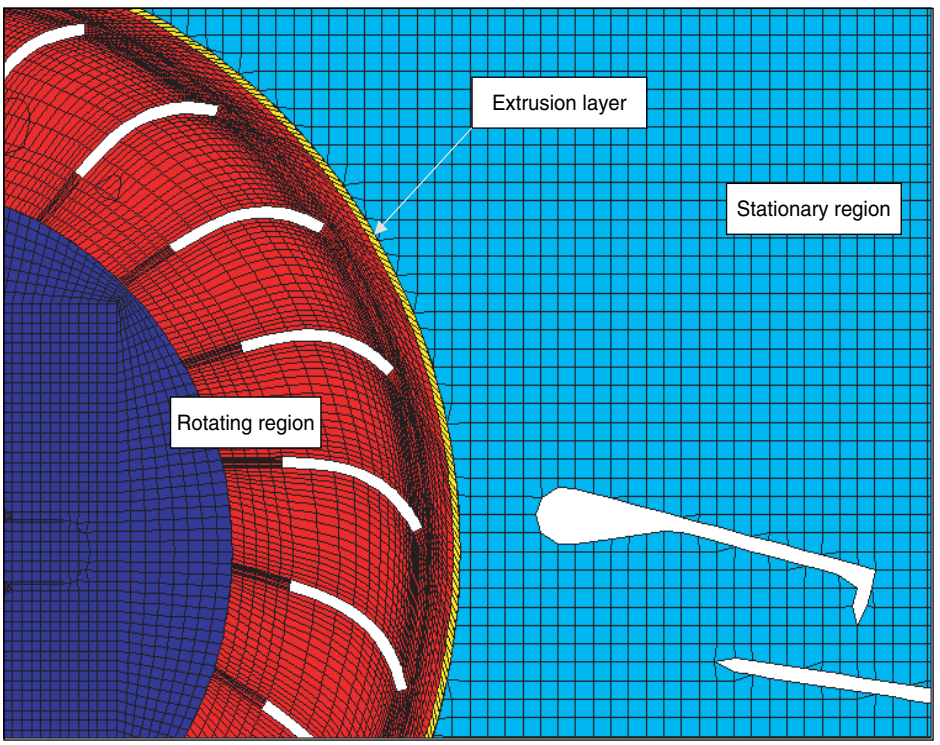

Figure 6 Detail of the computational grid in the region of the rotor with extrusion layer.

3.3 BOUNDARY CONDITIONS

All wetted surfaces were treated as impermeable, with hybrid wall functions applied (y+ independent). Fixed mass flow rates matching the experimental setup were applied to the front and rear inlets. The turbulence was assumed to have an intensity and length scale of 1% and 0,002 m respectively.

An atmospheric pressure boundary condition was applied at the exit of the exhaust channel. Turbulence parameters were calculated assuming a zero gradient along the streamlines intersecting the boundary.

Finally, the fan rotated at 1800 rpm. The steady state calculation used the implicit MRF approached to simulate the fan movement. The transient calculation explicitly rotated the cells that describe the fan and wheel using the moving mesh approach in STAR-CD.

3.4 TRANSIENT CALCULATIONS

The flow velocities, pressures and turbulence parameters in the domain were calculated using pressure-correction methods: SIMPLE for steady state and PISO for transient runs. With the SIMPLE method, and for a given pressure field, the discretised momentum equations are solved to obtain a “predicted” velocity field. The pressure field is then “corrected” so the continuity is satisfied. This corrected pressure is then used to correct the velocity field. The PISO algorithm is similar to the SIMPLE algorithm but has two corrector steps.

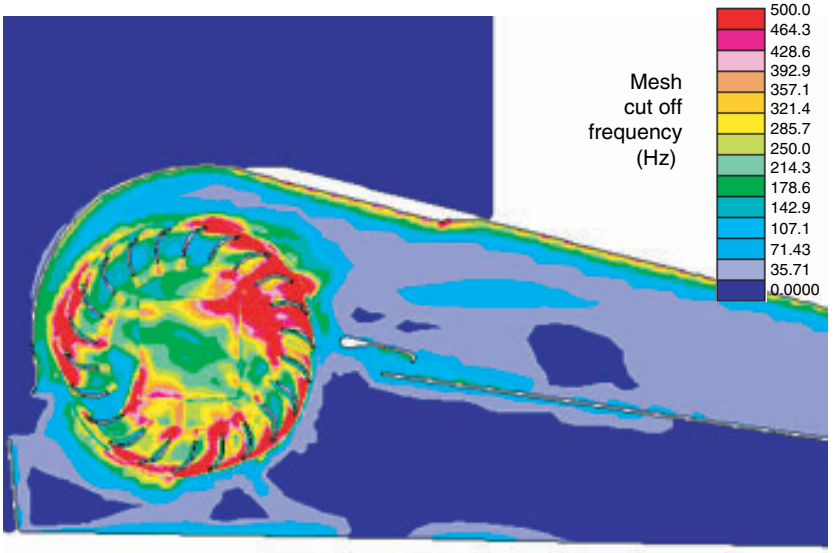

Figure 7 Frequency range captured by a first computational grid is hardly reaching 500 Hz in the fan region.

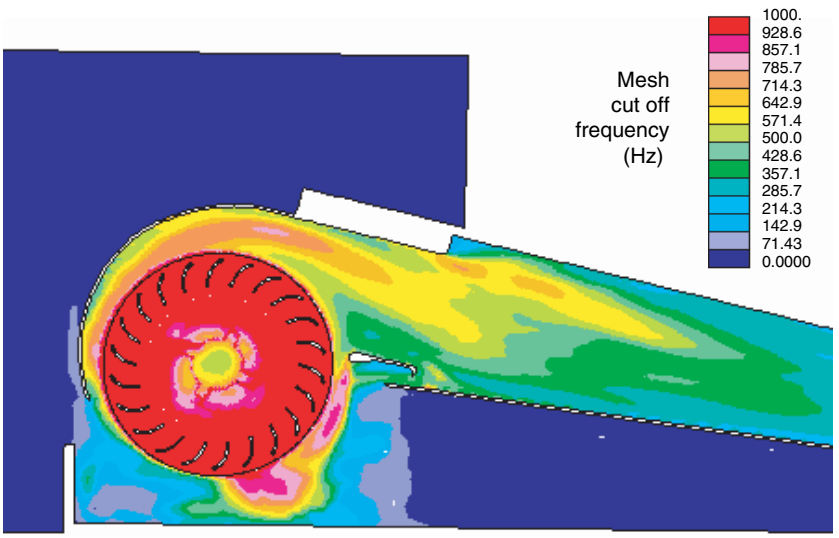

Figure 8 Frequency range captured by the final mesh exceeds 1 kHz in the fan and up to 700 Hz in the exhaust channel.

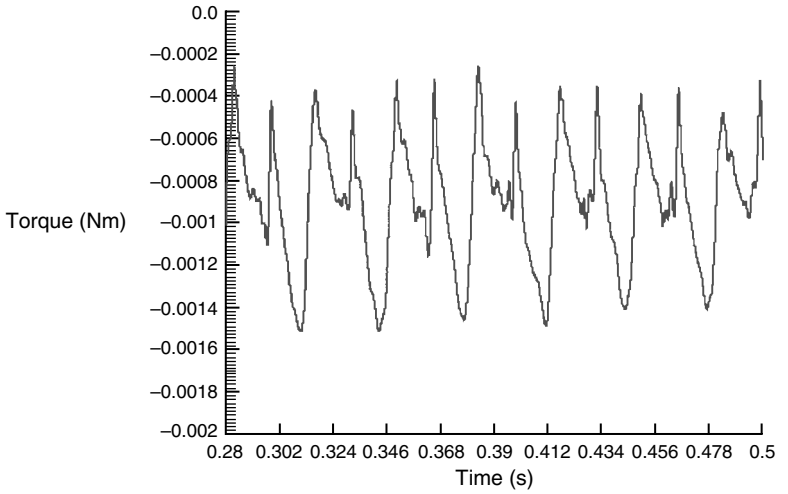

Figure 9 Torque monitoring on one single blade between 0.2 and 1.4 s.

A second-order MARS discretisation was used in the solution of the momentum equations. Euler-implicit temporal discretisation together with PISO was used.

A time step size of 7.215×10^{-5} s was used, which is equivalent to rotating one cell per time step. Attention to the mean and maximum Courant number showed that the restrictions applying to the Courant numbers when using PISO algorithm were satisfied.

The transient runs, started from an MRF steady state calculation, were run until a limit cycle state was reached. To assess the progress of the simulation, the torque on an individual blade was monitored (figure 9), as well as of the whole unit (figure 10). From the extract, it is clear that the behavior is periodic beyond a time of 0.22 s, approximately 6.5 revolutions. The torque on the fan unit began to oscillate around a mean value of 0.0192 N. The computations were kept running for a total of 15 revolutions.

3.5 ABOUT THE COUPLING METHOD BETWEEN THE CFD AND CA MODELS

The project is based on the coupling of the CFD code Star-CD 3.24 and the acoustic propagation code Actran. The planed coupling method is based on a control surface called 'porous boundary' [10]. Aerodynamic sources are defined on this surface, accounting for the effect of the flow enclosed inside the control surface on the noise generation. The divergence of the total stress tensor, given by, $\frac{\partial}{\partial x_j}(\rho v_i v_j + (p - p_0)\delta_{ij} - \tau_{ij})$ is computed. Here ρ is the density, p the pressure and τ_{ij} the viscous stress tensor. Subscript 0 on the pressure refers to a constant reference pressure.

With the present study, the porous boundary is idealized by a cylindrical surface located at a given radial distance from the edge of the fan blades.

The CFD model computes the divergence of the stress tensor on the control surface. The data are passed to the acoustic model that will propagate the noise sources. It is noticeable that the acoustic mesh is independent from the CFD grid, apart the control surface nodes that are common to both computational grids.

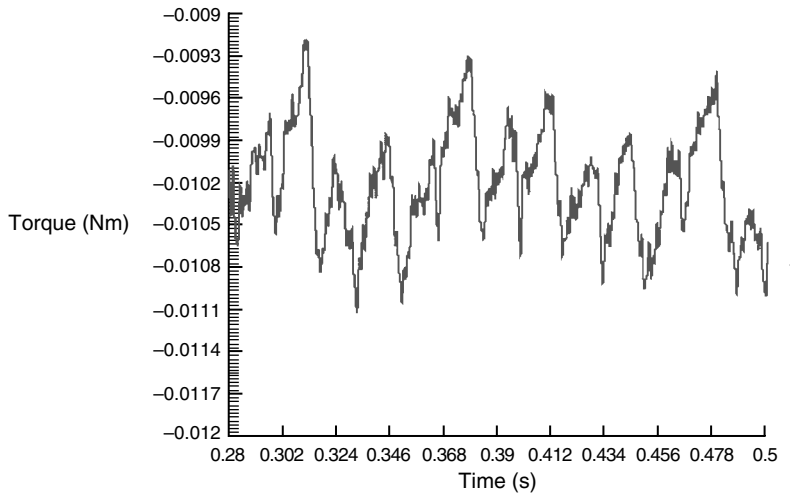

Figure 10 Torque on the fan unit between 0.2 and 1.4 s.

4. PARTICLE IMAGE VELOCIMETRY

4.1 THE PIV MEASUREMENT CHAIN

The Particle Image Velocimetry is an advanced measurement technique, which allows the simultaneous measurement of two or three components over a wide region of the flow field [11]. The flow under investigation, after being properly inseminated with fine particles (seeding), is illuminated on a plane by a laser sheet during successive instant. During the illumination periods, the light scattered by the particle tracers is recorded into an appropriate support – typically a CCD camera – and the images of the particles are then processed by a cross-correlation software able to recognize the particle displacement between two successive frames. The particle velocity is then directly determined once the time interval between the two exposures is known.

The PIV measuring chain of the University of Udine is a two dimensional PIV chain made of

- A 2 cavity pulsed Nd-Yag laser, capable to deliver 120 mJ per pulse in about 3 ns on a beam of 3 mm diameter,
- A digital camera at high resolution (1280 × 1024 pixels) and high sensitivity
- A timing unit to allow the correct synchronization of both laser and camera

The seeding is provided by a Laskin nozzle type seeding generator. It produces a vegetable oil aerosol with a mono-dispersed distribution around 1 m.

4.2 EXPERIMENTAL PROCEDURE

The tangential blower was tested at only one working condition: a fan revolution speed of 1800 rpm. Different sections were investigated to provide an exhaustive representation of the flow field but the present analysis will concentrate on the exhaust channel.

The reference system used for the experiments is given in figure 3. The X-axis of the reference system applied for the exhaust channel measurements was aligned with the duct centerline.

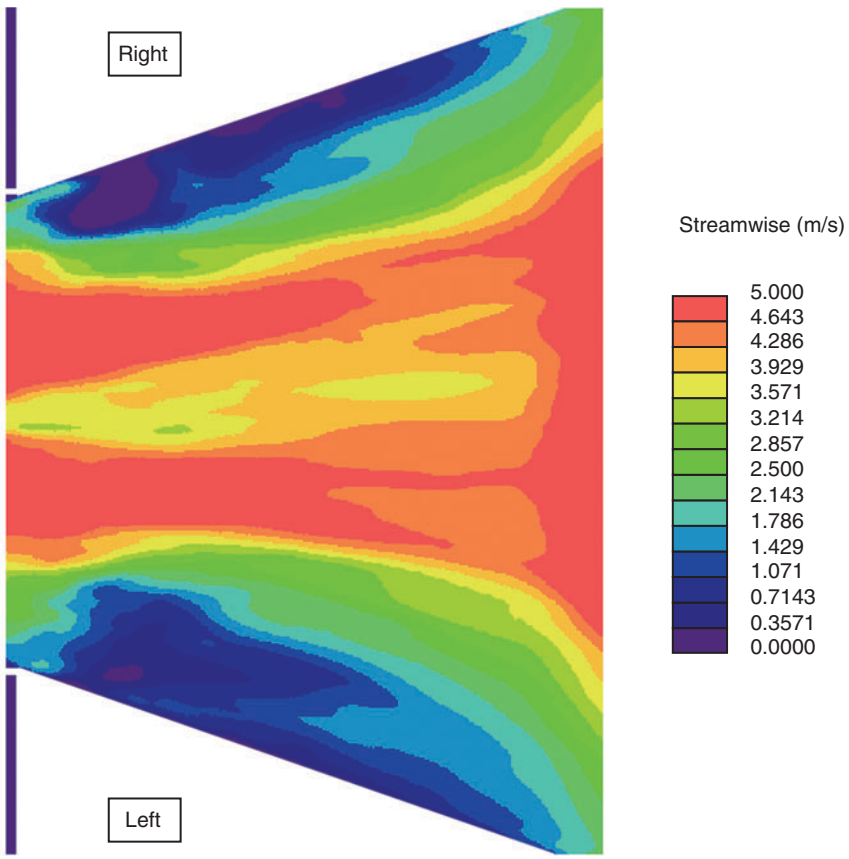

Figure 11 Contour of Stream-wise flow component in the exhaust duct computed by CFD.

4.3 PIV DATA INTERPRETATION

The experimental results presented in the next section are the ensemble averages of a given amount of instantaneous flow fields measured with PIV. Since the PIV measurements are not time-correlated due to the low frequency of acquisition (4 Hz), more information can be obtained from the analysis of an average flow field.

The number of samples to be used, in order to ensure the convergence of the statistics (namely the averaged and rms velocities), is mainly a function of the level of agitation of the flow [12]. In this particular application, the ensemble averages were obtained using 1000 samples.

The results here presented are affected by a measurement error that can be estimated in 3% in the instantaneous and mean velocity components and in 5% in the turbulent quantities.

5. RESULTS

5.1 QUALITATIVE ANALYSIS OF THE PIV RESULTS

The flow delivered from the fan volute to the exhaust duct is characterized by two separate jets of different strength (figure 12, streamwise component). Moving downstream, the two jets merge together and the flow exhibits an overall acceleration, according to the reduced cross section area of the duct.

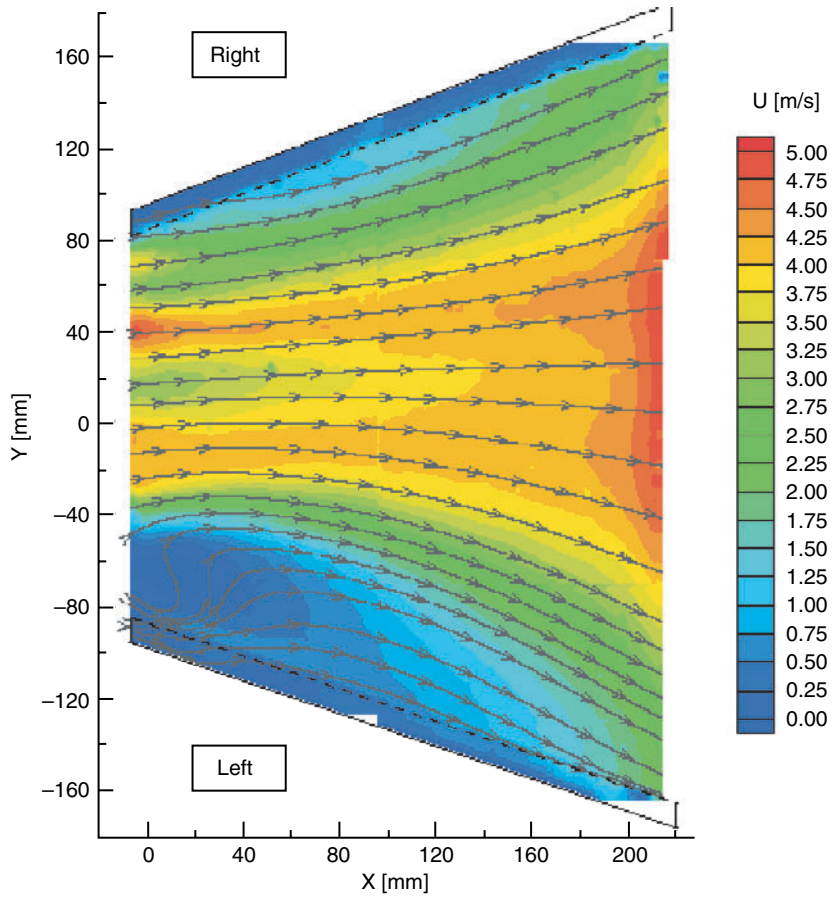

Figure 12 Contour of Stream-wise flow component in the exhaust duct measured by PIV.

The existence of two jets at the fan exit is justified:

- By the effect of the volute side walls, that imposes the no-slip condition on the external boundaries
- By the effect of the metal ring, that is located in the wheel centre plane and used to avoid deflection of the blades

The mean flow path is drawn toward one side (called right on figures) of the exhaust duct. On the opposite side, near the fan exit, there exists a strong recirculation area associated with the very low velocities. This asymmetry of the flow is due to the presence of the motor on one side of the casing.

The flow distribution computed by the CFD code results from averaging the flow quantities extracted during a complete fan revolution. The qualitative comparison between the numerical (figures 11 and 13) and experimental (figures 12 and 14 respectively) is fairly satisfying, the CFD model being able to reproduce the main features of the flow distribution.

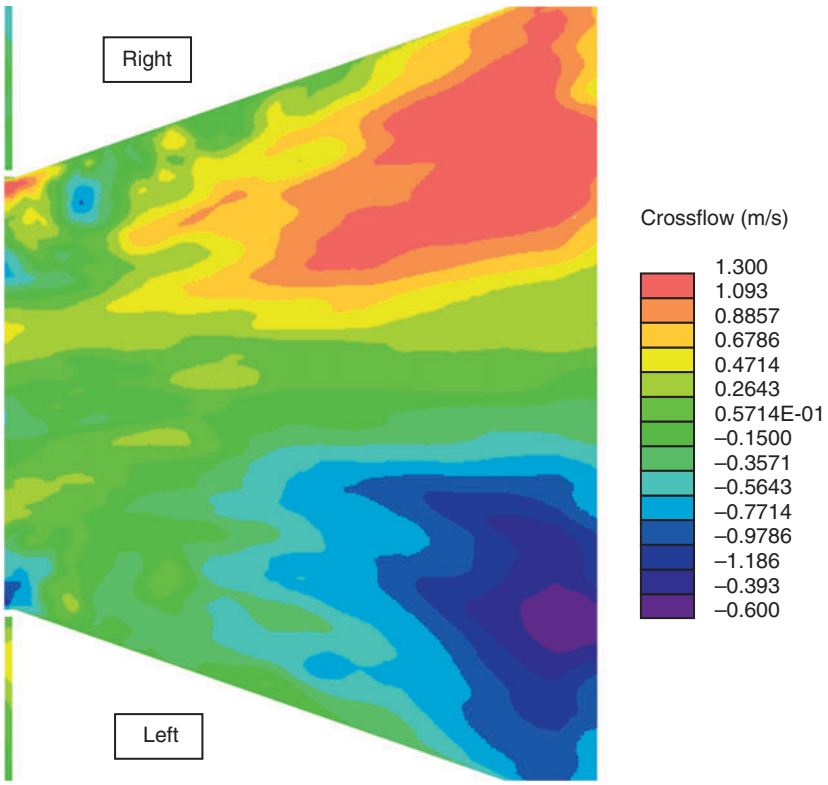

Figure 13 Contour of cross-wise flow component in the exhaust duct computed by CFD.

5.2 QUANTITATIVE RESULTS

For an objective comparison of the PIV and CFD results, velocity profiles have been compared at two locations X = 208 mm and X = 324 mm downstream the fan. The results are presented on figure 15 and 16.

A good match between the experimental and the computational results is observed with the CFD slightly over-predicting the flow speed at the first position (X = 208 mm). To verify the reliability of the fit a regression analysis has been performed to extract the R-squared value of a linear trend line (figure 17 and 18). This yields a value of $R^2 = 0.86$ at X = 208 mm and $R^2 = 0.94$ at X = 324 mm, confirming the good fitting of the curves.

The slight mismatch at X = 208 mm can be explained by the following reasons

- The exact position of the results plane can not be guaranteed
- In a region of high velocity gradients, a small error in the definition of the experimental data location can lead to significant velocity differences
- The time period used to extract the CFD data and calculate average quantities may be too short (484 samples).

The mismatch at X = 208 mm compared to X = 324 mm is explained by the fact the flow fluctuations are stronger at that level of the channel. At X = 324 mm, the height of the channel has reduced considerably and the flow tends to get more uniform vertical-wise.

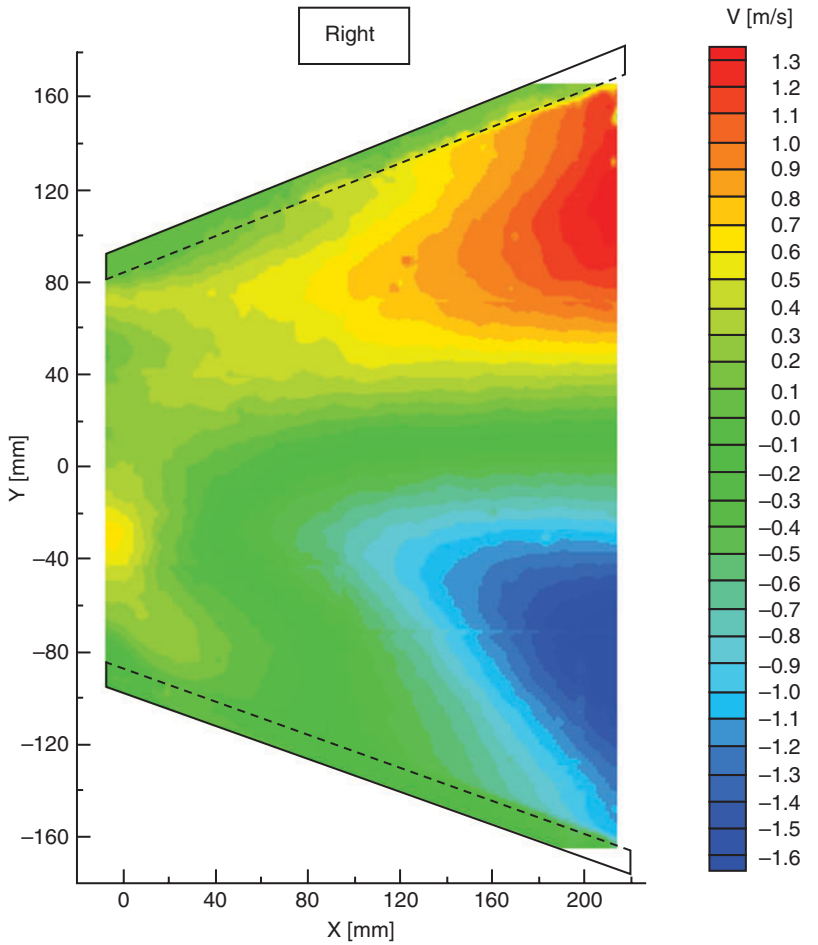

Figure 14 Contour of cross-wise flow component in the exhaust duct measured by PIV.

6. CONCLUSIONS

This paper was about the validation of the first step of a multiphysics analysis, coupling an Acoustic Software code with the CFD code STAR-CD in order to calculate the propagation and quantify the sound power levels generated by a tangential blower inside a duct system.

The time varying flow through a tangential blower was solved using the DES turbulence modeling and full moving mesh in STAR-CD. The flow distribution in the exhaust duct placed downstream the blower was compared with the advanced Particle Image Velocimetry technique. Good agreement was obtained between the extracted velocity profiles from the CFD model and the PIV results. Flow features such as a double jet and an asymmetry of the flow were observed experimentally and confirmed by the CFD computations. At this stage of the activity, the computations were considered validated and it was decided to initiate the following step of the aero-acoustic workflow i.e. to extract data from the CFD transient run and pass them to the acoustic code to resolve the acoustic propagation.

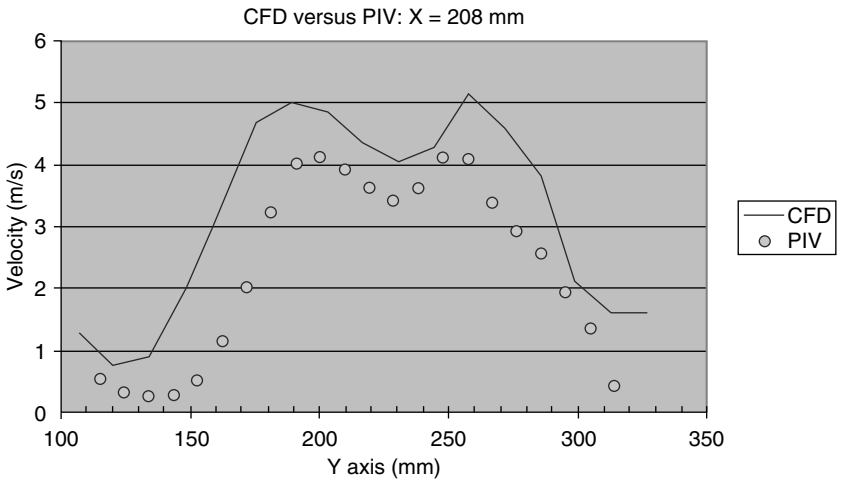

Figure 15 Streamwise velocity component profile : CFD versus PIV at X = 208 mm.

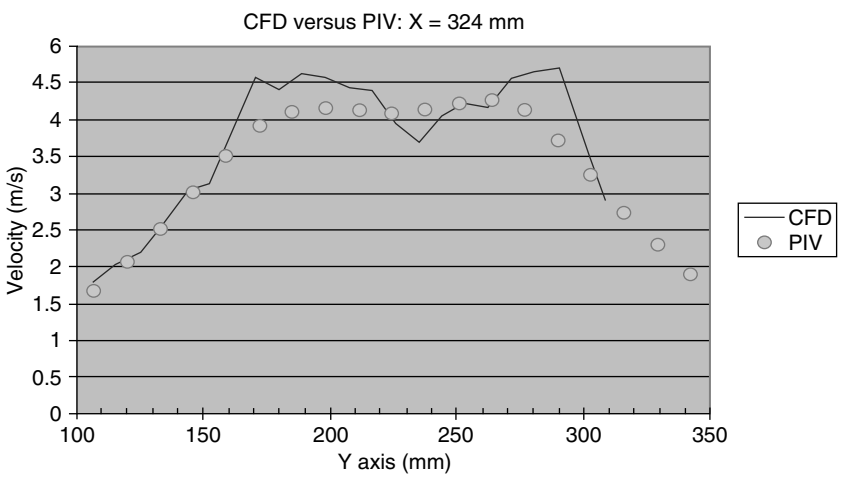

Figure 16 Streamwise velocity component profile : CFD versus PIV at X = 324 mm.

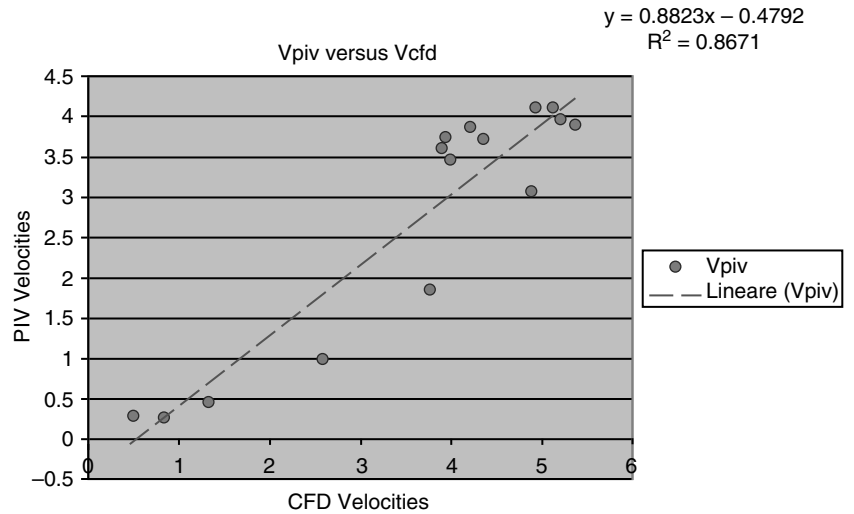

Figure 17 Linear regression fitting between CFD and PIV stream-wise velocity component at X = 208 mm.

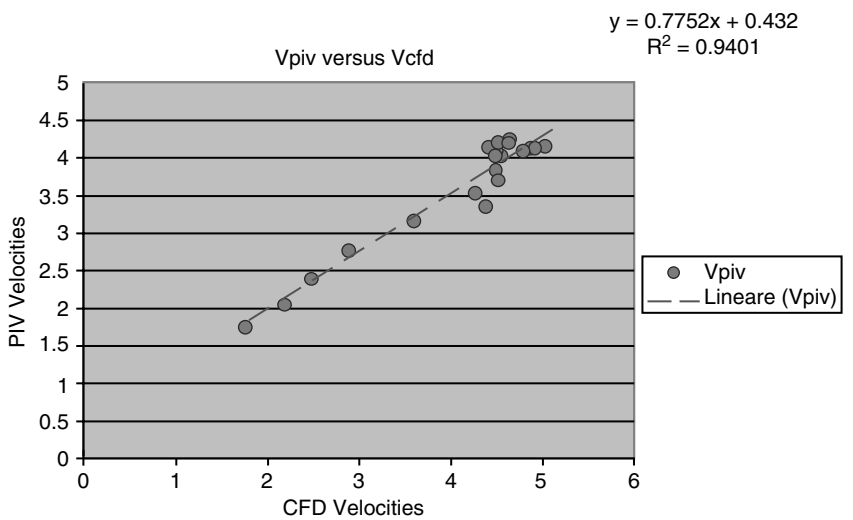

Figure 18 Linear regression fitting between CFD and PIV stream-wise velocity component at X = 324 mm.

REFERENCES

[1] Research for a Quieter Europe in 2020 – An Update Strategy Paper for the CALM Network – Oct. 2004.

[2] Lighthill "On sound generated aerodynamically" Proc. Roy. Soc. (London) Vol. A211, 1952.

[3] William K. Blake "Mechanics of Flow-induced Sound and Vibration – Volume 1: General Concepts and Elementary Sources" Ed. Academic Press, Inc 1986.

[4] W-H. JEON et al. "Analysis of unsteady flow field and aeroacoustic noise of an air-conditioner including cross flow fan", Fan Noise 2003 Proceedings.

[5] Alex Read et al. "Comparison between measured and predicted tonal noise from a subsonic fan using a coupled Computational Fluid Dynamics (CFD) and Computational Acoustics (CA) approach." AIAA 2004-2936.

[6] Mehmet çavuş et al. "Aeroacoustic Noise Prediction of an axial fan in a circular duct with LES" Ankara International Aerospace Conference -2005-092.

[7] F. Mendonca et al. "Towards understanding LES and DES for Industrial Aeroacoustic Predictions", International Workshop on 'LES for Acoustics', DLR Gottingen, Germany, 7–8th October 2002.

[8] G. Constantinescu "Handout: Large Eddy Simulation IV- Wall Models ^ Hybrid RANS-LES methods", 058:268 Turbulent Flows.

[9] Bakker A. "Sliding Mesh Simulation of Laminar Flow in Stirred Reactors", Published in "The Online CFM Book" at http://www.bakker.org/cfm - February 2000.

[10] S. Caro et al. "A New CAA Formulation based on Lighthill's Analogy applied to an Idealized Automotive HVAC Blower using AcuSolve and Actran/LA", AIAA2005-3015.

[11] Markus Raffel et al. "Particle Image Velocimetry: a practical guide", Springer, 1998.

[12] Riethmuller et al. "Measurements in Particulate Two Phase Flows", VKI Lecture Series 1981-3, Von Karman Institute for Fluid Dynamics, Belgium.